Two-photon-counting interferometry

Fabien Boitier,[1] Antoine Godard,[1] Nicolas Dubreuil,[2] Philippe Delaye,[2] Claude Fabre,[3] and Emmanuel Rosencher[1,4]
[1]*ONERA, The French Aerospace Lab, BP 80100, 91123 Palaiseau CEDEX, France*
[2]*Laboratoire Charles Fabry, Institut d'Optique, CNRS, Université Paris-Sud, Campus Polytechnique–RD 128, 91127 Palaiseau CEDEX, France*
[3]*Laboratoire Kastler Brossel, Université Pierre et Marie Curie–Paris 6, ENS, CNRS, CC74, 75252 Paris CEDEX, France*
[4]*Physics Department, Ecole Polytechnique–RD128, 91763 Palaiseau CEDEX, France*
(Received 16 June 2012; published 31 January 2013)

Two-photon-counting interferometry has been realized by measuring the electrical current due to two-photon absorption in the space-charge layer of a semiconductor detector located at the output port of an interferometer. We apply this technique to study the correlation properties of twin beams issued from parametric fluorescence. We describe in detail how the different second-order correlation functions (interbeam, intrabeam) can be extracted at the femtosecond time scale from raw data. The values of these correlation functions determined by our experiments are in excellent agreement with theory. More precisely, extrabunching in twin beams is unambiguously demonstrated and theoretically described using two models: a comprehensive multimode quantum optics model and a simpler classical stochastic approach. Given the high brightness of our twin-beam source, both theories yield similar results. Finally, convenient analytical expressions of the correlation functions were derived from both theories, expressions in which we have been able to relate specific terms to accidental and exact coincidences between photons. Two-photon interferometry thus determines to which extent twin photons are twin. This technique should become a useful tool for future quantum optics developments.

DOI: 10.1103/PhysRevA.87.013844 PACS number(s): 42.50.Ar, 42.65.Re, 42.50.Dv

I. INTRODUCTION

Since the first measurement by Hanbury-Brown and Twiss (HBT) [1], photon correlation properties have been important to numerous applications [2–11]. The HBT interferometry technique has been successfully extended to other fields, from neutron to cold atom interferometry [12,13], and has become a standard characterization tool in photonic applications such as quantum cryptography [14] or single-photon emission [15,16]. However, HBT time resolution is intrinsically limited by the single-photon detector response times, precluding the study of systems with coherence times smaller than a few hundred picoseconds [17].

As soon as the question of the simultaneity of the creation of twin-photon pairs by down-conversion was raised [18], circumventing this limitation became a major challenge for the quantum optics community [19,20]. The first correlation experiment with a resolution of a few tens of femtoseconds was inspired by an ultrashort pulse duration measurement technique based on second-harmonic generation (SHG) in a nonlinear crystal [21]. At this time this technique, hindered by an overall low quantum efficiency, has been overtaken by a novel approach based on two-photon interferences, the Hong-Ou-Mandel interferometer, which definitely demonstrated the quasisimultaneity of the creation of a single twin-photon pair [22].

Until the last decade, photon correlation studies have been primarily based on these two main techniques: the HBT interferometer—limited to light with long coherence time, and the Hong-Ou-Mandel Interferometer—limited to very low photon flux.

Since 2004, correlation measurement techniques based on nonlinear processes have been thoroughly revisited [23–26] and have provoked the photonics community to take a fresh look at photon-pair correlation measurement tools [27–37]. Indeed, the sensitivity of the technique based on SHG has been significantly improved by taking advantage of the high nonlinearity of periodically poled crystals and by capitalizing on the detector yield improvements [24].

In such experiments, photon pairs are sent on a beam splitter and then recombined in a SHG crystal. The second-order coherence properties are investigated by analyzing the SHG signal, and varying the delay between the two paths [25,27,28]. Since the SHG is a nearly instantaneous process, the temporal resolution of this photon correlation experiment can be as good as a few femtoseconds.

However, SHG in crystals has a very limited spectral acceptance. Consequently only the coincidences between photons belonging to the same pair [26], i.e., those which are phased matched, will be detected: As stated by Dayan [26], SHG "post-selects" photons of one pair. Appearing as an advantage in these experiments [24,25,27,28], this exclusive sensitivity to exact coincidences between twin photons actually prevents a complete investigation of the degree of correlation of such photon beams. More precisely, the amount of exact coincidences between twin photons cannot be rated relative to the amount of accidental coincidences originating from the chaotic nature of each of the beams (the signal and the idler ones). The effect of exact vs accidental coincidence (i.e., the simultaneity of twin-photon creation) thus cannot be easily explored.

Contrary to SHG or resonant two-photon absorption (TPA) in atoms [23,38–40], multiphoton processes in semiconductors—occurring between continua of energy—are not limited by phase matching or resonance conditions [41]. In 2009, it was experimentally demonstrated that two-photon counting (TPC) in a semiconductor detector allows the study of second-order correlations of broadband chaotic continuous-wave (cw) sources down to the microwatt level [42] and

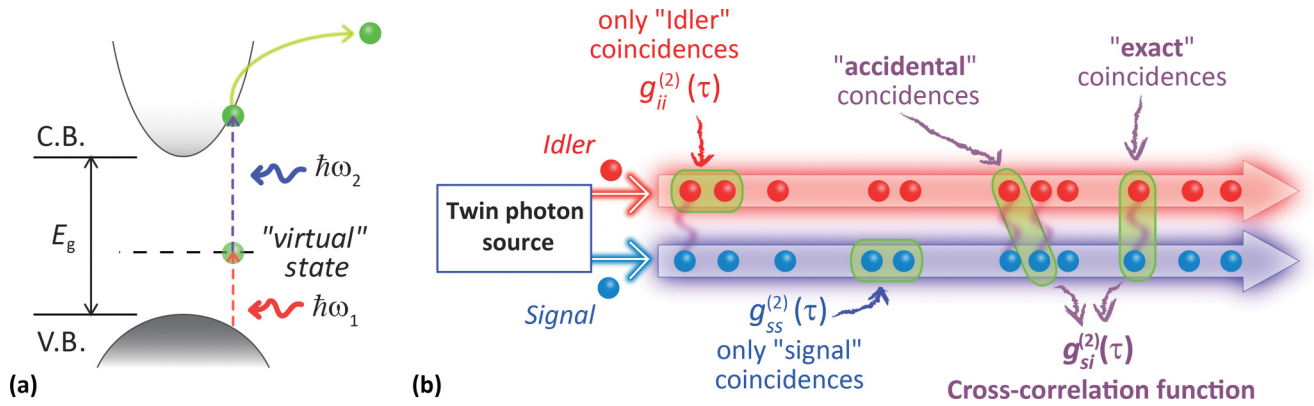

FIG. 1. (Color online) An intuitive overview of the two-photon-counting (TPC) principle: An electron in the valence band of a semiconductor is excited by a first photon (energy $\hbar\omega_1$) onto a "virtual state" in the band gap of the materials. The lifetime of the electron on this virtual state is determined by Heisenberg's second uncertainty principle, $\tau_H \approx \hbar/(E_g/2)$, i.e., in the femtosecond range. The electron will then be promoted into the conduction band by a second photon (energy $\hbar\omega_2$) inasmuch as (i) $\hbar\omega_1 + \hbar\omega_2 > E_g$ and (ii) the second photon reaches the electron within a delay smaller than the Heisenberg lifetime. TPC thus reveals the coincidences between photons within few femtoseconds (a). Different types of coincidence occur between the photons in twin beams: intrabeam accidental coincidences, interbeam accidental coincidences, and interbeam exact coincidences. All these coincidences will give rise to a TPC event. The purpose of this paper is to sort out the exact coincidences from the accidental ones (b).

also permits measurements of second-order correlation and cross-correlation functions of twin beams [43,44]. Moreover, this technique displays a unique capability to quantify the amount of pairs of twin photons compared to accidental coincidences. The purpose of this paper is to present a detailed description of TPC interferometry and to provide a theoretical background supporting the interpretation of our results.

II. TPC INTERFEROMETERS

A. An intuitive approach

Let us first provide an intuitive insight of how TPC is well adapted to the study of photon coincidence phenomena [see Fig. 1(a)]. Two photon beams ($\hbar\omega_1$ and $\hbar\omega_2$) are sent onto a semiconductor surface (of energy gap E_g). One photon of energy $\hbar\omega_x$ ($x = 1,2$) promotes an electron from the valence band to a virtual state in the band gap of the materials. The lifetime of the electron on this virtual state is roughly given by the Heisenberg lifetime $\tau_H \approx \hbar/\hbar\omega_x \approx \hbar/(\frac{1}{2}E_g)$, i.e., in the femtosecond range for semiconductors such as Si or GaAs. The electron will then be promoted onto the conduction band by a second photon inasmuch as (i) $\hbar\omega_1 + \hbar\omega_2 > E_g$ and (ii) the second photon reaches the electron within a delay smaller than the Heisenberg lifetime. At the end of this process, an electron-hole pair is produced which is ionized and swept out by the surface electric field of the space-charge region. In our experiment, the electron is emitted into vacuum, accelerated by a high electric field and induces an avalanche from several dynodes. An experimental evaluation of the quantum efficiency of the TPC is given in Appendix A.

Following our intuitive approach, the TPC signal is anticipated to be proportional to the expectation value of $\langle(1/\tau_H)\int_{-\tau_H}^{\tau_H} n(t)n(t+\tau)d\tau\rangle \approx \langle n(t)^2\rangle$, where $n(t)dt$ is the number of photons incident on the two-photon detector within time interval dt. In a quantum optics formulation, TPC values [45] are thus directly related to the expectation value of the operator $\hat{E}^{(-)}(t)\hat{E}^{(-)}(t)\hat{E}^{(+)}(t)\hat{E}^{(+)}(t)$ where $\hat{E}^{(+)}(t)$ and $\hat{E}^{(-)}(t)$ are the complex electric field operators and their Hermitian conjugates, respectively.

Now focusing on twin-photon beams (signal $\hbar\omega_s$ and idler $\hbar\omega_i$) generated by parametric down-conversion from pump photons (of energy $\hbar\omega_p$) in a nonlinear crystal, three different two-photon combinations can lead to a TPC event in a semiconductor [Fig. 1(b)]. Two of them occur at "degenerate" energy, i.e., $\hbar\omega_s + \hbar\omega_s$ or $\hbar\omega_i + \hbar\omega_i$, and one at nondegenerate energy, i.e., $\hbar\omega_s + \hbar\omega_i$.

An important point has to be highlighted at this stage. Any couple of photons $(\hbar\omega_s, \hbar\omega_i)$ such that $\hbar\omega_s + \hbar\omega_i > E_g$, is likely to be detected, even ones due to accidental coincidence, e.g., those for which $\hbar\omega_s + \hbar\omega_i \neq \hbar\omega_p$. Herein lies the key that distinguishes the TPC scheme from techniques such as SHG, or TPA in atomic systems, which post-select the $(\hbar\omega_s, \hbar\omega_i)$ couples for which resonance conditions (i.e., $\hbar\omega_s + \hbar\omega_i = \hbar\omega_p$) have to be met. These latter techniques cannot rate coherent vs incoherent pairs.

Suppose now that the total beam, consisting of the superposition of twin beams, is split into two sub-beams (by a beam splitter) and that one sub-beam is retarded by a delay τ relative to the other one. The two sub-beams are then recombined and sent on the TPC. The TPC signal recorded varying the delay τ is thus related to the autocorrelation of the whole parametric light, i.e., the superposition of the twin beams $(\hbar\omega_s, \hbar\omega_i)$; it will be referred to as "total autocorrelation signal." This TPC total autocorrelation signal involves different intensity correlation functions which can be expressed thanks to generalized second-order correlation functions [46]:

$$g^{(2)}_{lk}(\tau) = \frac{\langle \hat{E}^{(-)}_k(t)\hat{E}^{(-)}_l(t+\tau)\hat{E}^{(+)}_l(t+\tau)\hat{E}^{(+)}_k(t)\rangle}{\langle \hat{E}^{(-)}_k(t)\hat{E}^{(+)}_k(t)\rangle\langle \hat{E}^{(-)}_l(t)\hat{E}^{(+)}_l(t)\rangle}, \quad (1)$$

where k and l can stand for signal (s) or idler (i) and the involved light beams are supposed to be stationary.

Firstly, in TPC experiments, since the lifetime of a virtual state during the transition from valence to conduction band

states is extremely short, the process is intrinsically suitable for photon correlation studies at ultrashort time scales. Secondly, as schematically illustrated in Fig. 1(b), degenerate energy TPC events ($\hbar\omega_s + \hbar\omega_s$ or $\hbar\omega_i + \hbar\omega_i$) are linked to signal and idler self-correlation functions, respectively $g^{(2)}_{ss}(\tau)$ and $g^{(2)}_{ii}(\tau)$, whereas nondegenerate TPC events enable us to measure the photon cross-correlation between the signal and idler photons $g^{(2)}_{si}(\tau)$. We shall see below how our experimental setup independently determines these two contributions (self- and cross-correlation) to the TPC signal.

One should note that the cross-correlation function $g^{(2)}_{si}(\tau)$ may be interpreted as the normalized expectation $\langle n_i(t) n_s(t+\tau)\rangle / \langle n_s(t)\rangle\langle n_i(t)\rangle$. $g^{(2)}_{si}(\tau)$ is proportional to the probability of detecting a signal photon at $t+\tau$ once an idler photon has been detected at t (or the other way around): $g^{(2)}_{si}(\tau)$ thus determines to which extent twin photons are twin.

B. Experimental details

Two different setups are used, depending on which of the correlation functions among $g^{(2)}_{ss}(\tau)$, $g^{(2)}_{ii}(\tau)$, and $g^{(2)}_{si}(\tau)$ is considered. In both cases, the photon-pair source is based on spontaneous parametric down-conversion (SPDC) in a periodically poled lithium niobate (PPLN) nonlinear crystal (35 mm long). The phase matching is a type-0 one, meaning that the three polarizations (pump, signal, and idler) are the same [47]. The crystal is pumped by a mode-locked Ti:sapphire laser delivering 10-ps pulses at a repetition rate of 80 MHz. Averaged over many periods of the mode-locking cycles, the power of the photon-pair beam centered at 1.56 μm is about 50 μW for an average pump power of 2 W centered at 780 nm. This means that the peak power can reach a few tens of milliwatts. The quasi-phase-matching conditions are changed by tuning the temperature of the oven containing the PPLN crystal. Special attention is given to controlling and compensating for chromatic dispersion effects by the use of a SF14 glass prism pair setup as advised and demonstrated in Refs. [24,25,27,28]. It is now well known that high chromatic dispersion phenomena lead to the decoherence of the beams, which then display chaotic behaviors [27,28,43]. Finally, as shown in Refs. [43,44], the pulse duration is large compared to the coherence time of the source. Consequently, whenever the pulse intensity is nonzero, we can model it as a cw beam with a power equal to the pulse's peak power.

Figure 2 shows the experimental TPC interferometer used for the total autocorrelation measurement. We recall that the term "total" refers to the autocorrelation of the beam consisting of the superposition of the idler and signal beams. This first setup is based on a standard Michelson interferometer arrangement. The beam to analyze is sent on a 50/50 beam splitter. Sub-beams are then recombined after propagating over different optical paths before being focused by an aspherical lens on the GaAs photocathode of a photomultiplier tube (Hamamatsu H7421-50) [42–44,48]. A set of filters is placed in front of the detector to filter out any unwanted radiation with photon energy above the semiconductor band gap which would overwhelm the TPC signal. Adequate filtering is confirmed by verifying the quadratic dependence of the detector counts as a function of light intensity over eight orders of magnitude. The

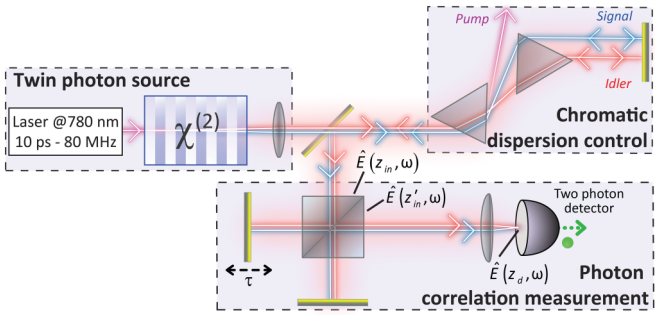

FIG. 2. (Color online) Michelson apparatus: The total beam consists of the superposition of the twin beams issued from the parametric down-conversion source. The total beam is split into two sub-beams by a beam splitter, one sub-beam being delayed by a motorized mirror. The two sub-beams are recombined and focused onto the two-photon counter. The TPC signal from the detector $S_2^{\text{Mich.}}(\tau)$ provides an interferogram from which the total autocorrelation function $g^{(2)}(\tau)$ is deduced. An apparatus controlling the chromatic dispersion allows dispersion effects to be studied.

focal spot diameter on the photocathode is about 5 μm. The TPC interferogram acquisition is carried out by translating a gold-coated mirror with a motorized translation stage while recording TPC at the same time. The TPC signal delivered by the detector, once properly normalized (see below) is the interferogram $S_2^{\text{Mich.}}(\tau)$. As detailed below (in Sec. II C), such an interferometer provides the first- and second-order correlation measurements [i.e., $g^{(2)}(\tau)$, $g^{(2)}_{ss}(\tau)$, $g^{(2)}_{ii}(\tau) g^{(2)}_{si}(\tau)$] of the total incident field.

When the field consisted of two distinct wavelengths, a second TPC apparatus, based on a Mach-Zehnder-like setup, was developed (Fig. 3). Its design is similar to the one used in Ref. [28], i.e., the two distinct wavelengths are separated by a dichroic mirror, propagated on different optical paths, recombined and focused onto the detection setup. No oscillatory features due to signal or idler self-interferences are involved. It is thus clear that only $g_{ss}(0), g_{ii}(0)$ and the cross-correlation function $g^{(2)}_{si}(\tau)$ are involved. In our case, the cutoff wavelength λ_{cut} of the dichroic mirror, i.e., the

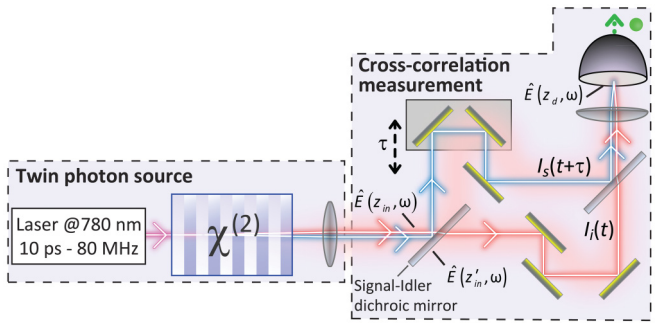

FIG. 3. (Color online) Mach-Zehnder-like apparatus. If the twin beams are nondegenerate, they can be separated by a dichroic mirror in two beams of different wavelengths. One of the beams is delayed relative to the other one by a motorized mirror. The beams are recombined and focused onto a two-photon counter. The TPC signal from the counter provides an interferogram $S_2^{MZ}(\tau)$ from which the cross-correlation $g^{(2)}_{si}(\tau)$ between the two beams is deduced.

wavelength below (respectively, above) which wavelengths are reflected (respectively, transmitted), is about 1.56 μm (twice the pump wavelength). The delay is varied by translating a mirror mount on the signal-wavelength path (see Fig. 3) and the detection setup is the TPC device previously described. The TPC signal delivered by the detector, once properly normalized (see below), is the interferogram $S_2^{MZ}(\tau)$.

C. What is measured in the Michelson apparatus?

As we are dealing with correlations which may have a quantum origin, it is better to use a quantized field approach from the beginning. The electric field of the radiation is described by the operator $\hat{E}^{(+)}(t)$ and can be expanded as a function of the single-frequency field operators $\hat{E}(z,\omega)$:

$$\hat{E}^{(+)}(t) = \frac{1}{\sqrt{2\pi}} \int_0^\infty d\omega\, \hat{E}(z,\omega) e^{-i\omega t}. \tag{2}$$

The electric field operator $\hat{E}(z_d,\omega)$ at the position z_d of the detector, situated at the output of the Michelson setup, can be linked to the operators $\hat{E}(z_{in},\omega)$ and $\hat{E}(z'_{in},\omega)$ defined at its two inputs by

$$\begin{aligned}\hat{E}(z_d,\omega) = \tfrac{1}{2}[i\eta(\omega)(1+e^{-i\omega\tau})\hat{E}(z_{in},\omega) \\ - \eta(\omega)(1-e^{-i\omega\tau})\hat{E}(z'_{in},\omega)].\end{aligned} \tag{3}$$

In this equation, $\eta(\omega) = e^{i\varphi(\omega)}$ is the phase factor which accounts for the dispersion experienced by the beams on their paths.

Considering that (i) a rather high-power field enters at input port z_{in} (>1 mW), (ii) only vacuum fluctuations enter at input port z'_{in}, and (iii) we are only dealing with intensity measurements, we can neglect the $\hat{E}(z'_{in},\omega)$ term in Eq. (3). We can therefore write the field operator at the detector in the time domain as the sum of the electric field operators at the output of each path of the interferometer:

$$\hat{E}^{(+)}(t) \approx \tfrac{1}{2}[\hat{E}_p^{(+)}(t) + \hat{E}_p^{(+)}(t+\tau)], \tag{4}$$

where $\hat{E}_p^{(+)}(t) = \frac{i}{\sqrt{2\pi}} \int_0^\infty d\omega\, \eta(\omega)\hat{E}(z_{in},\omega)e^{-i\omega t} \approx \bar{E}\,\hat{a}_p(t)$ is the "partial" operator describing each sub-beam. $\bar{E}$ is the mean electric field per photon (assuming a small enough frequency bandwidth) and $\hat{a}_p(t)$ is a photon annihilation operator in the time domain.

The intensity is then given by $\langle \hat{E}^{(-)}(t)\hat{E}^{(+)}(t)\rangle$ while the TPC signal is given by $\kappa\,\langle \hat{E}^{(-)}(t)\hat{E}^{(-)}(t)\hat{E}^{(+)}(t)\hat{E}^{(+)}(t)\rangle$ [46], κ being the two-photon absorption quantum yield (see Appendix A). In order to get rid of this quantum yield, one has to normalize the interferograms. As is usual in these two-photon absorption experiments [41], the normalization procedure is the following: The value of the TPC signal is measured when one arm of the interferometer is blocked [e.g., the $I(t)$ one in Fig. 2], and another value is measured when the other arm is blocked [e.g., the $I(t+\tau)$ one in Fig. 2]; the value of the normalizing quantity is the sum of these two values. It is straightforward to show that this normalizing quantity corresponds to $\frac{1}{8}\kappa\langle \hat{E}_p^{(-)}(t)\hat{E}_p^{(-)}(t)\hat{E}_p^{(+)}(t)\hat{E}_p^{(+)}(t)\rangle$.

Using this normalization procedure and expressing the output field operators in terms of their two time-delayed components [Eq. (4)], one can easily extend the classical formula of a normalized TPC interferogram $S_2^{\text{Mich.}}(\tau)$ [42,49,50]:

$$S_2^{\text{Mich.}}(\tau) = 1 + 2G^{(2)}(\tau) + 4\text{Re}[F^{(1)}(\tau)] + \text{Re}[F^{(2)}(\tau)], \tag{5}$$

where the functions $G^{(2)}(\tau)$, $F^{(1)}(\tau)$, and $F^{(2)}(\tau)$ are given by

$$G^{(2)}(\tau) = \frac{\langle \hat{a}_p^\dagger(t)\hat{a}_p^\dagger(t+\tau)\hat{a}_p(t+\tau)\hat{a}_p(t)\rangle}{\langle \hat{a}_p^\dagger(t)\hat{a}_p^\dagger(t)\hat{a}_p(t)\hat{a}_p(t)\rangle}, \tag{6}$$

$$F^{(1)}(\tau) = \frac{\langle \hat{a}_p^\dagger(t)\hat{a}_p^\dagger(t+\tau)\hat{a}_p(t+\tau)\hat{a}_p(t+\tau)\rangle + \langle \hat{a}_p^\dagger(t)\hat{a}_p^\dagger(t)\hat{a}_p(t)\hat{a}_p(t+\tau)\rangle}{2\langle \hat{a}_p^\dagger(t)\hat{a}_p^\dagger(t)\hat{a}_p(t)\hat{a}_p(t)\rangle}, \tag{7}$$

$$F^{(2)}(\tau) = \frac{\langle \hat{a}_p^\dagger(t)\hat{a}_p^\dagger(t)\hat{a}_p(t+\tau)\hat{a}_p(t+\tau)\rangle}{\langle \hat{a}_p^\dagger(t)\hat{a}_p^\dagger(t)\hat{a}_p(t)\hat{a}_p(t)\rangle}. \tag{8}$$

If the bandwidth of the optical spectrum is small compared to the carrier angular frequency ω_0 (with $\omega_0 = \omega_p/2$ for SPDC light), we can conveniently use the slowly varying time operator $\tilde{a}_p(t)$ in order to emphasize oscillating terms centered at ω_0 and $2\omega_0$:

$$\hat{a}_p(t) = \tilde{a}_p(t)e^{-i\omega_0 t}. \tag{9}$$

Equations (6)–(8) can thus be rewritten as follows:

$$G^{(2)}(\tau) = \frac{g^{(2)}(\tau)}{g^{(2)}(0)}, \tag{10}$$

$$F^{(1)}(\tau) = \frac{e^{-i\omega_0\tau}}{2g^{(2)}(0)} \frac{\langle \tilde{a}_p^\dagger(t)[\tilde{a}_p^\dagger(t)\tilde{a}_p(t) + \tilde{a}_p^\dagger(t+\tau)\tilde{a}_p(t+\tau)]\tilde{a}_p(t+\tau)\rangle}{\langle \tilde{a}_p^\dagger(t)\tilde{a}_p(t)\rangle^2}, \tag{11}$$

$$F^{(2)}(\tau) = \frac{e^{-i2\omega_0\tau}}{g^{(2)}(0)} \frac{\langle \tilde{a}_p^\dagger(t)\tilde{a}_p^\dagger(t)\tilde{a}_p(t+\tau)\tilde{a}_p(t+\tau)\rangle}{\langle \tilde{a}_p^\dagger(t)\tilde{a}_p(t)\rangle^2}, \tag{12}$$

where

$$g^{(2)}(\tau) = \frac{\langle \hat{a}_p^\dagger(t)\hat{a}_p^\dagger(t+\tau)\hat{a}_p(t+\tau)\hat{a}_p(t)\rangle}{\langle \hat{a}_p^\dagger(t)\hat{a}_p(t)\rangle^2}$$

is the second-order coherence function of the total incoming field.

Formulas (10)–(12) show that the experimental data contain a great deal of information about the incident fields:

(i) $F^{(1)}(\tau)$ (angular frequency ω_0 contribution) is reminiscent of a first-order correlation function of a Michelson interferometer.

(ii) $F^{(2)}(\tau)$ (angular frequency $2\omega_0$ contribution) is reminiscent of the optically nonlinear process involved in the two-photon detector.

(iii) $G^{(2)}(\tau)$ is a slowly varying function which contains the second-order correlation function between the two beams. *It can thus be obtained by filtering out the high-frequency contribution from the interferogram* leading to $S_2^{LPF}(\tau) = 1 + 2G^{(2)}(\tau)$.

One may note that, as is well known in the usual pulse duration measurement [41], $S_2^{\text{Mich.}}(0) = 8$. Moreover, assuming that all field intensities are uncorrelated at long delay times, the total second-order correlation function $g^{(2)}(\tau)$ can be directly deduced from the experimental interferogram:

$$g^{(2)}(\tau) = \frac{S_2^{LPF}(\tau) - 1}{S_2^{LPF}(\infty) - 1}. \tag{13}$$

D. What is measured in the Mach-Zehnder apparatus

The field operator calculated at the two-photon detector position (see Fig. 3) is given as a function of the fields at the input by an analog of Eq. (3) for the Michelson setup:

$$\hat{E}(z_d,\omega) = \{\eta_i(\omega)\xi(\omega) - \eta_s(\omega)[1-\xi(\omega)]e^{-i\omega\tau}\}\hat{E}(z_{in},\omega) + i\sqrt{\xi(\omega)[1-\xi(\omega)]}[1-e^{-i\omega\tau}]\hat{E}(z'_{in},\omega), \tag{14}$$

where $\eta_{s,i}(\omega)$ accounts for the chromatic dispersion experienced by the beam on the path i or s from the source output to the TPC detector and $\xi(\omega)$ is the transmission coefficient of the dichroic mirror at the angular frequency ω (see Fig. 3). Once again, one can neglect the effect of the vacuum fluctuation entering on the other input port z'_{in}. Assuming in addition that the dichroic mirror has a perfect cutoff frequency $\omega_{cut} = \omega_p/2$, the output field operator in the time domain can be written as

$$\hat{E}^{(+)}(t) \approx \bar{E}[\hat{a}_s(t+\tau) + \hat{a}_i(t)], \tag{15}$$

where the signal and idler time dependent annihilation operators, $\hat{a}_s(t)$ and $\hat{a}_i(t)$, are expanded as a function of the single-frequency field operators $\hat{E}(z,\omega)$ in type 0 phase matching conditions as follows:

$$\hat{a}_s(t) = \frac{i}{\bar{E}\sqrt{2\pi}}\int_{\omega_p/2}^{\omega_p} d\omega\, \eta(\omega)\hat{E}(z_{in},\omega)e^{-i\omega t} = \tilde{a}_s(t)e^{-i\omega_s t}, \tag{16}$$

$$\hat{a}_i(t) = \frac{i}{\bar{E}\sqrt{2\pi}}\int_{0}^{\omega_p/2} d\omega\, \eta(\omega)\hat{E}(z_{in},\omega)e^{-i\omega t} = \tilde{a}_i(t)e^{-i\omega_i t}. \tag{17}$$

$\tilde{a}_s(t)$ and $\tilde{a}_i(t)$ are the corresponding slowly varying time operators with ω_s and ω_i the central angular frequencies for signal and idler, respectively.

From these expressions and using a similar normalization procedure as for the Michelson apparatus, i.e., normalized by $\kappa(\langle \hat{E}_s^{(-)}\hat{E}_s^{(-)}\hat{E}_s^{(+)}\hat{E}_s^{(+)}\rangle + \langle \hat{E}_i^{(-)}\hat{E}_i^{(-)}\hat{E}_i^{(+)}\hat{E}_i^{(+)}\rangle)$ evaluated a time t, one finds that the TPC signal in the present Mach-Zehnder configuration is given by

$$S_2^{MZ}(\tau) = 1 + \frac{4\langle \hat{a}_i^\dagger(t)\hat{a}_s^\dagger(t+\tau)\hat{a}_s(t+\tau)\hat{a}_i(t)\rangle}{\langle \hat{a}_s^\dagger(t)\hat{a}_s^\dagger(t)\hat{a}_s(t)\hat{a}_s(t)\rangle + \langle \hat{a}_i^\dagger(t)\hat{a}_i^\dagger(t)\hat{a}_i(t)\hat{a}_i(t)\rangle}, \tag{18}$$

which can be rewritten in terms of the correlation functions defined in Eq. (1) as

$$S_2^{MZ}(\tau) = 1 + 4g_{si}^{(2)}(\tau) \times \frac{\langle \hat{a}_s^\dagger(t)\hat{a}_s(t)\rangle\langle \hat{a}_i^\dagger(t)\hat{a}_i(t)\rangle}{g_{ss}^{(2)}(0)\langle \hat{a}_s^\dagger(t)\hat{a}_s(t)\rangle^2 + g_{ii}^{(2)}(0)\langle \hat{a}_i^\dagger(t)\hat{a}_i(t)\rangle^2}. \tag{19}$$

Let us note that the constant 1 in Eqs. (18) and (19) originates from zero-delay self-interference terms $g_{ss}(0)$ and $g_{ii}(0)$.

Therefore the intensity cross-correlation function $g_{si}^{(2)}(\tau)$ can be directly obtained from the present signal [46] by

$$g_{si}^{(2)}(\tau) = \frac{S_2^{MZ}(\tau) - 1}{S_2^{MZ}(\infty) - 1}. \tag{20}$$

III. EXPERIMENTAL TPC INTERFEROGRAMS

A. Autocorrelation measurements using Michelson TPC

Figures 4(a)–4(d) show the experimental TPC interferograms of the twin beams obtained using the Michelson apparatus, under different conditions of chromatic dispersion and phase matching of the SPDC source. The beam spectra are shown in the insets on the right. The left insets are closeups of the interferogram at long delays. Each TPC response is normalized using the procedure described above, i.e., by the sum of each TPC generated by photons from one path while the other is blocked.

In the cases of Figs. 4(a) and 4(b), the two beams are altered by high chromatic dispersion at degeneracy and far from degeneracy, respectively. In both cases, no distinguishable features are observed in the insets on the left. The main difference between these two interferograms is the modulation observed in the thick red curve at the center of Fig. 4(b). This modulation occurring at the $(\omega_s - \omega_i)$ frequency in the nondegenerate case will be explained in Sec. IV A. In such conditions where chromatic dispersion is not compensated, one can note that, at degeneracy, the TPC interferogram is equivalent to the one obtained with chaotic sources [42,43].

In the cases of Figs. 4(c) and 4(d), chromatic dispersion phenomena are carefully compensated. The modulation at $(\omega_s - \omega_i)$ still occurs and is more clearly visible. The main difference between these two figures and Figs. 4(a) and 4(b) is the onset of fast oscillations at long time delays [see left insets in Figs. 4(a)–4(d)]. In order to analyze this spectral component, a time-frequency analysis is carried out.

Figure 5 shows the result of this time-frequency analysis, i.e., a plot of the frequency components of the TPC

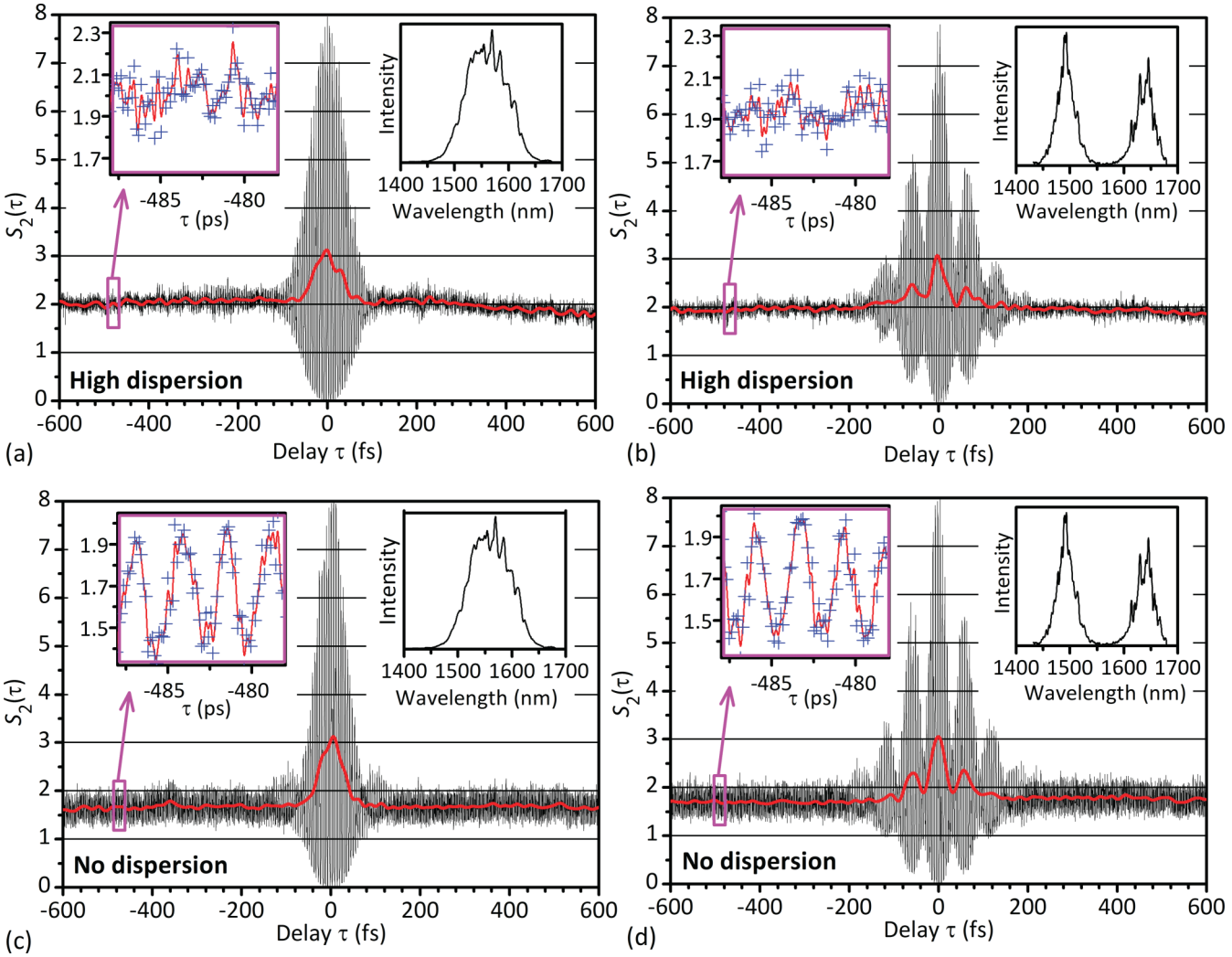

FIG. 4. (Color online) Experimental TPC interferograms of the twin beams obtained with the Michelson apparatus of Fig. 2. The thin gray curves in the central part of the figures are the raw interferograms with no data processing. The thick red curve is obtained by low-frequency filtering of the thin gray curves. The second-order correlation function $g^{(2)}(\tau)$ is deduced from this thick red curve. The right insets show the spectrum of the incident beam. The left insets are a closeup of the interferograms at long delay. These four panels map the following situations: (a) degenerate beams, no dispersion compensation; (b) nondegenerate beams, no dispersion compensation; (c) degenerate beams, dispersion compensation; (d) nondegenerate beams, dispersion compensation.

interferogram as a function of the delay τ (spectrogram), *in the nondegenerate case* [Fig. 4(d)]. Many features may be observed in this figure where one can easily distinguish the spectral contents of functions $G^{(2)}(\tau)$ [or $g^{(2)}(\tau)$] at low frequency [Eq. (6)], $F^{(1)}(\tau)$ centered at $\omega_p/2$ [Eq. (11)], and $F^{(2)}(\tau)$ centered at ω_p [Eq. (12)].

Firstly, one can notice that the spectral content of $g^{(2)}(\tau)$ is only visible for short delays ($\tau < 200$ fs) and contains a modulation term at $(\omega_s - \omega_i)$ which is observed for correlated as well as uncorrelated lights [see Figs. 4(d) and 4(b)]. The origin of such features is discussed in Sec. IV.

As for $g^{(2)}(\tau)$, the contribution of $F^{(1)}(\tau)$ is only visible for short delays. It mainly consists of two spectral components at ω_s and ω_i, whose origin is also discussed in Sec. IV.

The spectral content of $F^{(2)}(\tau)$ is more remarkable: Besides second harmonics ($2\omega_s$ and $2\omega_i$) also visible at short delays only, an additional component appears at the pump frequency ω_p [see also left inset in Figs. 4(c) and 4(d)] and does not vanish for very long delay. This long-lasting oscillation at the pump frequency was previously observed with other techniques [25, 44,51–53]. It is related to the particular coherence of the whole photon field due to the coherence imposed by the pump field as discussed in Sec. IV B4.

Second-order correlation functions can be finally extracted from these interferograms by filtering out high frequencies and using Eq. (13). Figure 6 shows $g^{(2)}(\tau)$ of several sources emitting around 1.55 μm and obtained using this technique: a cw laser, a chaotic source [from Fig. 4(a)], and a degenerate photon-pair source displaying the same spectral content as the chaotic one [from Fig. 4(c)]. Let us recall that, by simply adjusting the dispersion compensation setup, we can continuously tune our source from highly correlated twin beams (Fig. 2) to two independent chaotic ones. The distinction between these three sources is unambiguously underlined by the experimental value of $g^{(2)}(0)$: 1 for laser, 2 for chaotic source, and 3 for twin beams. This latter extrabunching can

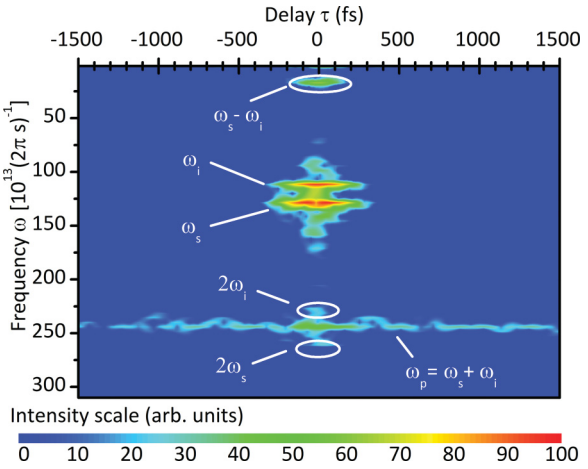

FIG. 5. (Color online) Time-frequency analysis (i.e., the spectral content of the signal as a function of the delay τ) of the interferogram in Fig. 4(d).

intuitively be linked to the additional exact coincidences of photons from the same pair as illustrated in Fig. 1(b) [44,46].

At this stage, it might be useful to remember that, though the rough interferograms for the chaotic [Fig. 4(a)] and the twin beams [Fig. 4(c)] display the same value at zero delay, the deduced second-order correlation functions are different since the long term behaviors $[S^{(2)}_{LPF}(\infty)]$ are different [see Eq. (13)].

B. Nondegenerate biphoton cross-correlation measurements using the Mach-Zehnder apparatus

Finally, the cross-correlation functions $g^{(2)}_{si}(\tau)$ were directly measured thanks to the modified Mach-Zehnder setup when signal and idler wavelengths can be conveniently separated, i.e., in the nondegenerate case.

Figures 7(a) and 7(b) show $g^{(2)}_{si}(\tau)$ obtained with the use of Eq. (20). One notes that $g^{(2)}_{si}(0) = 2$ in contrast to $g^{(2)}_{si}(0) = 1$ for independent beams. This striking behavior is another

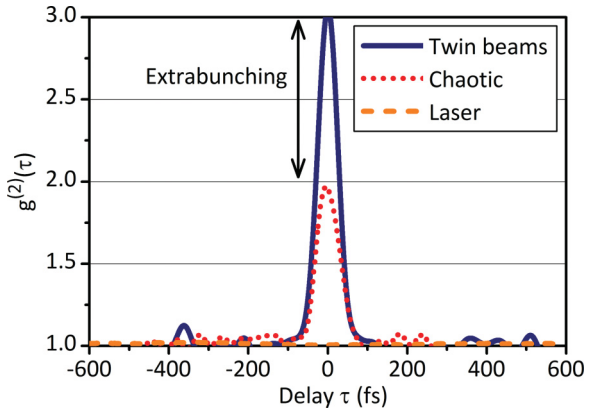

FIG. 6. (Color online) Second-order correlation functions $g^{(2)}(\tau)$ of several sources emitting around 1.55 μm obtained by filtering out Michelson TPC data: a cw laser, a chaotic source [from Fig. 4(a)], and a photon-pair source with the same spectral content as the chaotic source [from Fig. 4(c)].

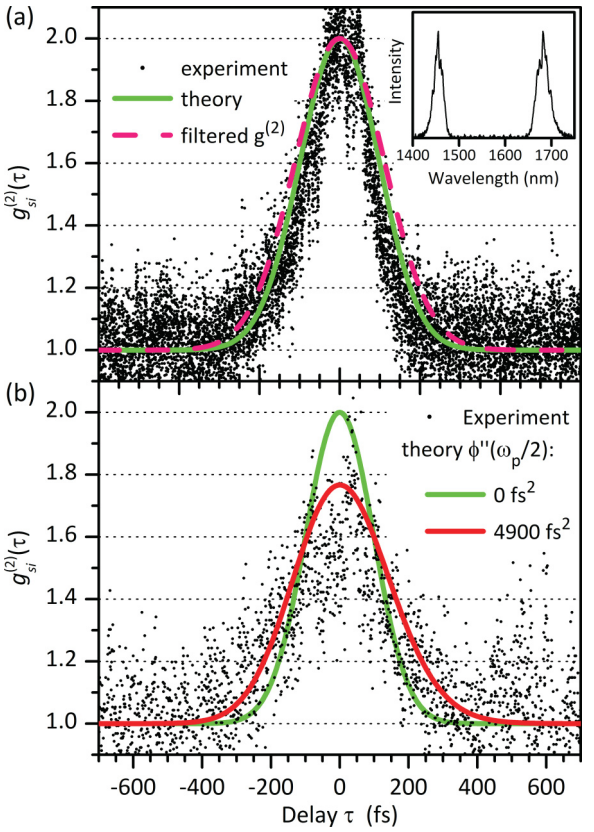

FIG. 7. (Color online) Cross-correlation $g_{si}(\tau)$ measurements by the Mach-Zehnder apparatus of Fig. 3: (a) with no dispersion and (b) altered by a dispersive element on the beam path. Red dashed curve in (a) is extracted from the Michelson apparatus results of Fig. 4(d) using Eqs. (21)–(23).

clear signature of additional exact coincidences between the twin-beam photons. The signal and idler wavelengths are, respectively, centered at 1.45 and 1.69 μm (inset). In Fig. 7(a), chromatic dispersion phenomena are well compensated whereas in Fig. 7(b)), the group delay dispersion—the second derivative of the spectral phase—evaluated at the degeneracy frequency $\varphi''(\omega_p/2)$ is about 4900 fs^2 (adding a dispersive element on the beam path).

These results quantitatively demonstrate the correlations existing between the signal and idler photons within an equivalent coherence time of 200 fs and confirm the expected chromatic dispersion sensitivity [27,28,43].

In order to conveniently describe these striking results of TPC interferograms, it is clear that the peculiar coherence properties between signal and idler beams have to be taken into account. This is developed in the next section.

IV. INTERPRETATION OF EXPERIMENTAL RESULTS

A. Intra- and interbeam contributions

The total second-order correlation function $g^{(2)}(\tau)$ can be easily related to the signal-signal, idler-idler, and signal-idler correlation functions from Eqs. (1), (16), and (17) through

$$g^{(2)}(\tau) = g^{(2)}_{\text{intra}}(\tau) + g^{(2)}_{\text{inter}}(\tau), \tag{21}$$

where $g^{(2)}_{\text{intra}}(\tau)$ and $g^{(2)}_{\text{inter}}(\tau)$ are two different kinds of contributions in the $g^{(2)}$ function:an *intrabeam* one,

$$g^{(2)}_{\text{intra}}(\tau) = \tfrac{1}{4}\big[g^{(2)}_{ss}(\tau) + g^{(2)}_{ii}(\tau)\big], \tag{22}$$

and an *interbeam* one,

$$g^{(2)}_{\text{inter}}(\tau) = \frac{1}{2}\left(g^{(2)}_{si}(\tau) + 4\text{Re}\left\{e^{-i(\omega_i-\omega_s)\tau} \times \frac{\langle\tilde{a}^{\dagger}_s(t+\tau)\tilde{a}^{\dagger}_i(t)\tilde{a}_i(t+\tau)\tilde{a}_s(t)\rangle}{\langle[\tilde{a}^{\dagger}_s(t)+\tilde{a}^{\dagger}_i(t)][\tilde{a}_s(t)+\tilde{a}_i(t)]\rangle^2}\right\}\right). \tag{23}$$

In these equations, $g^{(2)}_{ss}$, $g^{(2)}_{ii}$, and $g^{(2)}_{si}$ are nonoscillating functions while the last term in the interbeam contribution oscillates at the angular frequency $(\omega_s - \omega_i)$. This explains the $(\omega_s - \omega_i)$ modulation observed in Figs. 4 and 5.

Equation (23) shows that $g^{(2)}_{si}(\tau)$ (see Sec. III B) may also be obtained from the Michelson apparatus by filtering out the $\omega_s - \omega_i$ oscillating term from the interbeam correlation function $g^{(2)}_{\text{inter}}(\tau)$. This result is shown in Fig. 7(a) and compares well with the result of the Mach-Zehnder apparatus.

B. Calculation of the photon correlation functions from the twin-beam properties

Our aim is now to relate our observations to the correlation properties of the SPDC source. Experimental results show that we clearly need to introduce in our theoretical description the chromatic dispersion effects and the fact that the SPDC light contains twin photons.

Given the low quantum yield of two-photon absorption and the dark count rate (28 s^{-1}), the typical power involved in our experiments is rather high (photon flux peak value $\Phi \sim 10^{18}\ s^{-1}$). Since the bandwidth of the beams is $\Delta \approx 10^{14}\ s^{-1}$, the number of photons per mode is high ($\sim 10^4$). We are then in a situation where quantum correlation effects are involved in intense beams, a situation reminiscent of the "twin beams" generated by optical parametric oscillators above threshold which display strong quantum intensity correlations [54]. In the present case, though the quantum description of the phenomenon is by far the most satisfying and simple one, a semiclassical description of the phenomenon is also possible and proposed in Appendix B.

1. *Description of the parametric down-conversion process*

A general description of SPDC second-order correlation and its application to a narrow-bandwidth "two-photon detector" (SFG or TPA in atoms) can be found in Ref. [26]. Here, we mainly aim at theoretically underlining the interest of a large two-photon detection bandwidth. Moreover, since we deal with a large number of photons per mode, simplifications may be introduced, leading to simple expressions, the physics of which may be easily captured. The following detailed description is based on a continuous-variable description of creation and annihilation operators [26,43,46,55].

The photon-pair annihilation operator $\hat{a}(z_e,\omega)$ at the output of the nonlinear crystal can be expressed by means of crystal entrance operators $\hat{a}(\omega)$ and $\hat{a}^{\dagger}(\omega_p - \omega)$:

$$\hat{a}(z_e,\omega) = [\mu(\omega)\hat{a}(\omega) + i\,\nu(\omega)\hat{a}^{\dagger}(\omega_p - \omega)] \times \exp\{i[\Delta k(\omega)/2 + k(\omega)]L\}. \tag{24}$$

In this equation, $k(\omega)$ is the wave vector at angular frequency ω and $\Delta k(\omega)$ is the quasi-phase-mismatch parameter in the periodically poled crystal given by

$$\Delta k(\omega) = k(\omega_p) - k(\omega) - k(\omega_p - \omega) - \frac{2\pi}{\Lambda}, \tag{25}$$

where Λ is the poling period of the PPLN crystal. L is the crystal length. Finally, the parametric interaction propagation factors $\mu(\omega)$ and $\nu(\omega)$ are given by the formulas [55]

$$\mu(\omega) = \cosh[\gamma(\omega)L] - i\frac{\Delta k(\omega)}{2\gamma(\omega)}\sinh[\gamma(\omega)L], \tag{26}$$

$$\nu(\omega) = \frac{g(\omega)}{\gamma(\omega)}\sinh[\gamma(\omega)L], \tag{27}$$

where the parametric gain $g(\omega)$ can be obtained from the incident pump intensity I_p, the effective nonlinear coefficient d_{eff} (16 pm/V), the speed of light c, and the vacuum impedance Z_0 (=377 Ω):

$$g(\omega) = \frac{d_{\text{eff}}}{c}\sqrt{\frac{2\omega[\omega_p - \omega]Z_0 I_p}{n(\omega)n(\omega_p - \omega)n(\omega_p)}}, \tag{28}$$

and $\gamma(\omega)$ is the effective parametric gain:

$$\gamma(\omega) = \sqrt{g(\omega)^2 - \Delta k(\omega)^2/4}. \tag{29}$$

As the experimental down-converted spectrum ($\geqslant$ 50 nm) and TPC (~600 nm) bandwidths are much broader than the pump bandwidth (~0.06 nm), we neglected the latter and considered an infinitely-narrow-band pump at the angular frequency ω_p. Let us note that due to the intrinsic symmetry of the type 0 generation process, signal and idler propagation factors are equal, i.e., $\mu(\omega) = \mu(\omega_p - \omega)$ and $\nu(\omega) = \nu(\omega_p - \omega)$.

2. *A generalized expression of the interbeam first-order correlation function* $g^{(1)}_{si}(\tau)$

By expanding the signal-idler cross correlation function [Eq. (1)] thanks to Eq. (24) and using the well-known commutation rule [46],

$$[\hat{a}(\omega),\hat{a}^{+}(\omega')] = \delta(\omega - \omega'), \tag{30}$$

a tedious but straightforward derivation (see Appendix C) [56] enables us to write $g^{(2)}_{si}(\tau)$ for twin beams as

$$g^{(2)}_{si}(\tau) = 1 + \left|g^{(1)}_{si}(\tau)\right|^2, \tag{31}$$

which is somewhat similar to the result obtained for chaotic beams [46]. In Eq. (31), we introduce the following first-order cross-correlation function defined as

$$g^{(1)}_{si}(\tau) = \frac{\langle e^{-i\,\varphi_0}\tilde{a}_s(t+\tau)\tilde{a}_i(t)\rangle e^{-i\omega_s\tau}}{\sqrt{\langle\tilde{a}^{\dagger}_s(t)\tilde{a}_s(t)\rangle\langle\tilde{a}^{\dagger}_i(t)\tilde{a}_i(t)\rangle}} = \frac{1}{2\pi\sqrt{\phi_s\phi_i}}\int_{\omega_p/2}^{\omega_p} d\omega\,\eta(\omega)\eta(\omega_p - \omega)\nu(\omega)\mu(\omega)e^{-i\,\omega\tau}. \tag{32}$$

In this equation, $\varphi_0 = [k(\omega_p) - \frac{2\pi}{\Lambda}] + \frac{\pi}{2}$ is a convenient constant phase factor and ϕ_s (respectively, ϕ_i) is the signal

(respectively, idler) photon flux given by [46]

$$\phi_s = \frac{1}{2\pi}\int_{\omega_p/2}^{\omega_p} d\omega\,|\eta(\omega)\nu(\omega)|^2,$$
$$\phi_i = \frac{1}{2\pi}\int_{0}^{\omega_p/2} d\omega\,|\eta(\omega)\nu(\omega)|^2. \tag{33}$$

The signal-idler first-order cross-correlation function $g_{si}^{(1)}(\tau)$ describes the coherence of the photon-pair field relative to the pump one. It is linked to the idler-signal function by $g_{si}^{(1)}(\tau) = e^{-i\omega_p\tau} g_{is}^{(1)}(-\tau)$. Two other properties have to be noticed here: (i) $|g_{si}^{(1)}(\tau)|$ can be higher than 1, and (ii) such a function is sensitive to chromatic dispersion as opposed to usual first-order correlation function of cw sources.

3. *Second-order correlation function $g^{(2)}(\tau)$ of twin beams*

By introducing Eq. (24) into Eq. (23) and carrying out the derivation in the same way as detailed in Appendix C for the calculation of Eq. (31), the interbeam contribution can now be expressed by use of a first-order correlation functions

$$g_{\text{inter}}^{(2)}(\tau) = \frac{1}{2} + \frac{1}{2}\text{Re}\left[g_{ss}^{(1)}(\tau)g_{ii}^{(1)*}(\tau)\right] + \frac{\left|g_{si}^{(1)}(\tau) + g_{is}^{(1)}(\tau)\right|^2}{4}, \tag{34}$$

where $g_{ss}^{(1)}(\tau)$ [respectively, $g_{ii}^{(1)}(\tau)$] is the signal (respectively, idler) first-order correlation function:

$$g_{ss}^{(1)}(\tau) = \frac{1}{2\pi\phi_s}\int_{\omega_p/2}^{\omega_p} d\omega\,|\eta(\omega)\nu(\omega)|^2 e^{-i\omega\tau},$$
$$g_{ii}^{(1)}(\tau) = \frac{1}{2\pi\phi_i}\int_{0}^{\omega_p/2} d\omega\,|\eta(\omega)\nu(\omega)|^2 e^{-i\omega\tau}. \tag{35}$$

To illustrate the scope of Eq. (34), one can analyze its value at zero delay. In this case, $g_{ss}^{(1)}(0) = g_{ii}^{(1)}(0) = 1$ and $g_{\text{inter}}^{(2)}(\tau) = 1 + \frac{1}{4}|g_{si}^{(1)}(0) + g_{is}^{(1)}(0)|^2$. We recover here the value of "1" if the two chaotic sources are independent, whereas the last term $[\frac{1}{4}|g_{si}^{(1)}(0) + g_{is}^{(1)}(0)|^2]$ describes the peculiar properties of the twin-beam correlations.

We are thus proposing the following interpretation of Eq. (34). The two first terms of the right-hand side (i.e., $\{1 + \text{Re}[g_{ss}^{(1)}(\tau)g_{ii}^{(1)*}(\tau)]\}/2$) are related to "accidental" coincidences due the chaotic behavior of the source. The third term, [i.e., $|g_{si}^{(1)}(\tau) + g_{is}^{(1)}(\tau)|^2/4$] is the coherent part due to the exact coincidences between the photons of a same pair [26,43]. It is easy to see that, compared to a chaotic source, this last term is responsible for the biphotons' "extrabunching" parameter which leads to $g^{(2)}(0) > 2$, as schematically illustrated in Fig. 1(b).

To highlight the terms where the carrier frequencies ω_s and ω_i are involved, let us introduce the slowly varying envelopes of the correlation functions defined as

$$g_{jk}^{(1)}(\tau) = \tilde{g}_{jk}^{(1)}(\tau)e^{-i\omega_k\tau}. \tag{36}$$

The intra- and interbeam second-order correlation functions can then be rewritten as

$$g_{\text{intra}}^{(2)}(\tau) = \tfrac{1}{2} + \tfrac{1}{4}\left[\left|\tilde{g}_{ss}^{(1)}(\tau)\right|^2 + \left|\tilde{g}_{ii}^{(1)}(\tau)\right|^2\right], \tag{37}$$

and

$$g_{\text{inter}}^{(2)}(\tau) = \frac{1}{2} + \frac{\left|\tilde{g}_{si}^{(1)}(\tau)\right|^2 + \left|\tilde{g}_{si}^{(1)}(\tau)\right|^2}{4} + \frac{1}{2}\text{Re}\left\{\left[\tilde{g}_{ss}^{(1)}(\tau)\tilde{g}_{ii}^{(1)*}(\tau) + \tilde{g}_{is}^{(1)}(\tau)\tilde{g}_{si}^{(1)*}(\tau)\right] \times e^{-i(\omega_s-\omega_i)\tau}\right\}. \tag{38}$$

One thus recovers the oscillation at $\omega_s - \omega_i$ angular frequency that is observed in Figs. 4 and 5. One could also note that these oscillations exist even if the fields are not mutually coherent, which is experimentally observed. The term "quantum beating" usually given to this term may be somewhat misleading. It is related to the indistinguishable nature of the paths taken by each photon [57].

4. *First- and second-order correlation oscillating functions*

To complete the TPC interferogram modeling, it remains to calculate the two contributions $F^{(1)}(\tau)$ and $F^{(2)}(\tau)$ introduced in Eqs. (7) and (8). These functions are calculated in the same way as for Eqs. (21), (31), and (34), and are, respectively, given by

$$F^{(1)}(\tau) = \frac{1}{g^{(2)}(0)}\left\{g_{ss}^{(1)}(\tau) + g_{ii}^{(1)}(\tau) + \frac{g_{si}^{(1)}(0)}{4}\left[g_{si}^{(1)*}(-\tau) + g_{is}^{(1)*}(-\tau)\right] + \frac{g_{si}^{(1)*}(0)}{4}\left[g_{si}^{(1)}(\tau) + g_{is}^{(1)}(\tau)\right]\right\}, \tag{39}$$

$$F^{(2)}(\tau) = \frac{1}{2g^{(2)}(0)}\left\{\left[g_{ss}^{(1)}(\tau) + g_{ii}^{(1)}(\tau)\right]^2 + 2\left|g_{si}^{(1)}(0)\right|^2 e^{-i\omega_p\tau}\right\}. \tag{40}$$

As done with Eqs. (37) and (38), Eqs. (39) and (40) can be rewritten in terms of slowly varying envelope correlation functions:

$$F^{(1)}(\tau) = \frac{1}{g^{(2)}(0)}\left\{\left[\tilde{g}_{ss}^{(1)}(\tau) + \frac{\tilde{g}_{si}^{(1)}(0)}{4}\tilde{g}_{is}^{(1)*}(-\tau) + \frac{\tilde{g}_{si}^{(1)*}(0)}{4}\tilde{g}_{is}^{(1)}(\tau)\right]e^{-i\omega_s\tau} + \left[\tilde{g}_{ii}^{(1)}(\tau) + \frac{\tilde{g}_{si}^{(1)}(0)}{4}\tilde{g}_{si}^{(1)*}(-\tau) + \frac{\tilde{g}_{si}^{(1)*}(0)}{4}\tilde{g}_{si}^{(1)}(\tau)\right]e^{-i\omega_i\tau}\right\}, \tag{41}$$

$$F^{(2)}(\tau) = \frac{1}{2g^{(2)}(0)}\left\{\left[\tilde{g}_{ss}^{(1)}(\tau)\right]^2 e^{-2i\omega_s\tau} + \left[\tilde{g}_{ii}^{(1)}(\tau)\right]^2 e^{-2i\omega_i\tau} + 2\left[\tilde{g}_{ss}^{(1)}(\tau)\tilde{g}_{ii}^{(1)}(\tau) + \left|\tilde{g}_{si}^{(1)}(0)\right|^2\right]e^{-i\omega_p\tau}\right\}. \tag{42}$$

It is clear from Eq. (39) that the first-order correlation functions $g^{(1)}(\tau)$ can be extracted from the measurement of $F^{(1)}(\tau)$.

We shall now show how Eqs. (40)–(42) explain the experimental results of Figs. 4 and 5. One notes from Eq. (41) that $F^{(1)}(\tau)$ contains only terms oscillating at carrier angular frequencies ω_s and ω_i. These oscillations exist inasmuch as the different first-order correlation functions $\tilde{g}^{(1)}_{xy}(\tau)\,(x,y=s,i)$ are nonzero, i.e., within the coherence time.

Equations (40) and (42) show that for a chaotic source, the contribution $F^{(2)}(\tau)$ is proportional to the square of the first-order correlation function of the total field $g^{(1)}(\tau) = g^{(1)}_{ss}(\tau) + g^{(1)}_{ii}(\tau)$, leading to oscillating terms at angular frequencies $2\omega_s$, $2\omega_i$, and ω_p. Oscillations at $2\omega_s$ and $2\omega_i$ exist inasmuch as $\tilde{g}^{(1)}_{ss}(\tau)$ and $\tilde{g}^{(1)}_{ii}(\tau)$ are nonzero. Similarly, oscillations at ω_p exist inasmuch as $\tilde{g}^{(1)}_{ss}(\tau)\tilde{g}^{(1)}_{ii}(\tau)$ is nonzero [we recall that $\tilde{g}^{(1)}_{si}(0) = 0$ for mutually incoherent beams]. These oscillations are thus present for delays shorter than the coherence time of the chaotic source.

In the case of a twin-beam field, an additional term appears, proportional to $|g^{(1)}_{si}(0)|^2$ and oscillating at the pump frequency ω_p in our case. This oscillation persists during the whole pump pulse duration [25,44,58,59].

C. "High-gain" regime

Taking into account our experimental conditions (high-gain regime), some further simplifications can be made. The phase-mismatch parameter $\Delta k(\omega)$ can be neglected compared to the parametric gain $g(\omega)$. This assumption leads to the well-known propagation factor approximation in Eqs. (26) and (27):

$$\mu(\omega) \approx \nu(\omega) \approx \tfrac{1}{2}\exp[g(\omega)z_c]. \tag{43}$$

Moreover, as the chromatic dispersion is compensated by a prism pair setup, the dispersion factor $\eta(\omega)$ is equal to 1. The first-order cross-correlation functions $[g^{(1)}_{si}(\tau)$ and $g^{(1)}_{is}(\tau)]$ are thus equal to their respective first-order correlation function: $g^{(1)}_{ss}(\tau) = g^{(1)}_{si}(\tau) = g^{(1)*}_{si}(-\tau)$ and $g^{(1)}_{ii}(\tau) = g^{(1)}_{is}(\tau) = g^{(1)*}_{is}(-\tau)$ [see Eqs. (32) and (35)].

Using the above approximations, the components of interferograms given in Eqs. (21), (39), and (40) are found to be

$$g^{(2)}(\tau) = 1 + \frac{\left|g^{(1)}_{ss}(\tau) + g^{(1)}_{ii}(\tau)\right|^2}{2}, \tag{44}$$

$$F^{(1)}(\tau) = \frac{g^{(1)}_{ss}(\tau) + g^{(1)}_{ii}(\tau)}{2}, \tag{45}$$

$$F^{(2)}(\tau) = \frac{\left[g^{(1)}_{ss}(\tau) + g^{(1)}_{ii}(\tau)\right]^2}{6} + \frac{e^{-i\omega_p\tau}}{3}. \tag{46}$$

Equation (44) shows that for high gain and if the dispersion is zero, the $g^{(2)}(0)$ value is 3 $[g^{(1)}_{ss}(0) = g^{(1)}_{ii}(0) = 1]$. Of course, values higher than 3 can be obtained at lower gain. So as to emphasize the specificities of twin beams vs chaotic light, let us write the corresponding expressions of $g^{(2)}(\tau)$, $F^{(1)}(\tau)$, and $F^{(2)}(\tau)$ for uncorrelated beams $[g^{(1)}_{si}(\tau) = 0]$. Thereby, Eqs. (21), (39), and (40) become

$$g^{(2)}_{\text{chao.}}(\tau) = 1 + \frac{\left|g^{(1)}_{ss}(\tau) + g^{(1)}_{ii}(\tau)\right|^2}{4}, \tag{47}$$

$$F^{(1)}_{\text{chao.}}(\tau) = \frac{g^{(1)}_{ss}(\tau) + g^{(1)}_{ii}(\tau)}{2}, \tag{48}$$

$$F^{(2)}_{\text{chao.}}(\tau) = \frac{\left[g^{(1)}_{ss}(\tau) + g^{(1)}_{ii}(\tau)\right]^2}{4} = \left[F^{(1)}_{\text{chao.}}(\tau)\right]^2. \tag{49}$$

As already highlighted, a first obvious difference between twin beams and uncorrelated light can be seen when one compares the $g^{(2)}(\tau)$ and $g^{(2)}_{\text{chao.}}(\tau)$ expressions given by Eqs. (44) and (47). Indeed, even in the high-gain "classical" regime, there is an unequivocal extrabunching effect linked to the twin character of the beams, i.e., $g^{(2)}(0) = 3$ while $g^{(2)}_{\text{chao.}}(0) = 2$.

On the other hand, the expressions of the interferogram components $F^{(1)}(\tau)$ are identical for the twin beams [see Eq. (45)] and the chaotic beams [see Eq. (48)]. This is not surprising since $F^{(1)}(\tau)$ describes the first-order coherence properties. Consequently chaotic and twin beams with identical spectral content will display the same interferogram component $F^{(1)}(\tau)$. TPC interferometry thus provides a simultaneous measurement of the first-order coherence function $g^{(1)}(\tau)$ from which the spectral content of the beams may be determined by the Wiener-Khintchine theorem.

Even in the high-gain regime, the second-order oscillating function $F^{(2)}(\tau)$ still exhibits the discriminating features discussed in the previous subsection concerning Eq. (40). The study of $F^{(2)}(\tau)$ thus provides an alternative way to recover the specific properties of twin beams, i.e., the evaluation of the extrabunching correlation term $|g^{(1)}_{si}(0)|^2$ [here with $|g^{(1)}_{si}(0)|^2 = 1$] and the determination of the biphoton coherence properties.

Figure 8 shows the TPC interferogram modeling using Eq. (5) and Eqs. (34)–(40) without further approximation. All the physical parameters used in Eqs. (24)–(29) have been experimentally determined so that no adjustable parameters have been used. The agreement between experiment (Fig. 4) and theory (Fig. 8) is excellent.

V. CONCLUSION

In this paper, we have described and theoretically backed up in detail the operation principles of two-photon-counting interferometry. This technique is shown to offer drastic advantages compared to those of SHG: (i) It is more convenient since no phase matching condition is required and (ii) it is a nonresonant technique so that accidental as well as exact photon coincidences can be detected and rated relative to each other. Moreover it provides a huge detection bandwidth, allowing the correlation properties to be determined at the femtosecond time scale. Using this experimental configuration, different light beams have been investigated: lasers, blackbody, and twin beams issued from parametric down-conversion. Photon bunching in blackbody chaotic sources [i.e., $g^{(2)}(0) = 2$] as well as photon extrabunching in bright twin beams [i.e., $g^{(2)}(0) = 3$], either degenerate or nondegenerate, have been

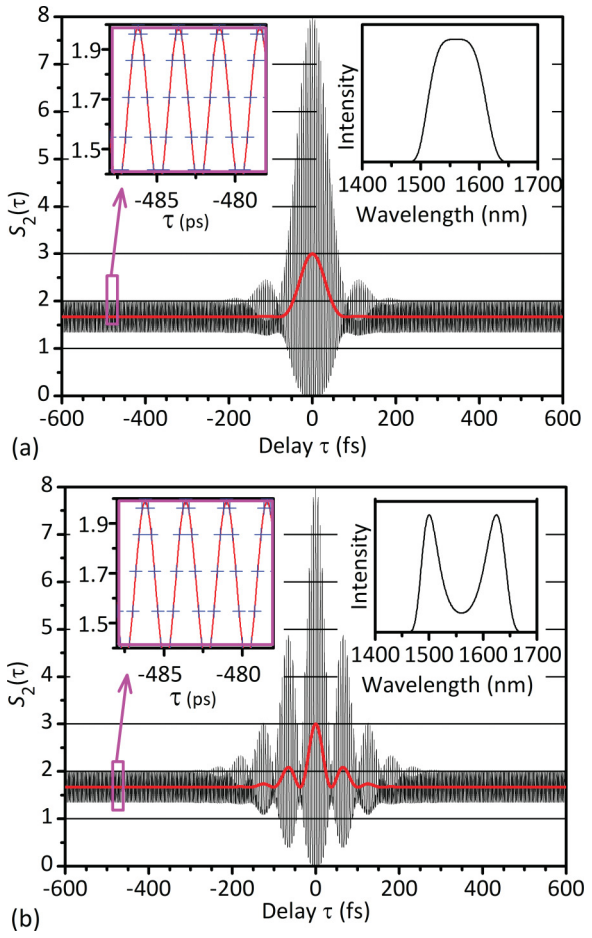

FIG. 8. (Color online) Modeling of the TPC interferograms corresponding to the experimental conditions of (a) Fig. 4(c) and (b) Fig. 4(d). The quantum model is described in Sec. IV.

unambiguously demonstrated at the femtosecond time scale. We have described how these results could be intuitively explained in terms of accidental and exact coincidences between pairs of photons.

We have shown how and which second-order correlation parameters can be extracted from our measurements, particularly the cross-correlation function between two beams $g_{si}^{(2)}(\tau)$ but also intrabeam $g_{\text{intra}}^{(2)}(\tau)$ and interbeam $g_{\text{inter}}^{(2)}(\tau)$ ones. Using a quantum optics theory as well as a stochastic semiclassical approach, we have been able to find relations between these correlation terms and attribute specific terms to accidental and exact coincidences between photons. Theoretical models (either based on the quantum or stochastic approach) are in excellent agreement with our experimental results, with no adjustable parameters. Particularly, all the features appearing in the time-frequency analysis of our TPC spectra are thoroughly explained and used for the determination of the different second-order correlation functions.

This technique could also be applied to the determination of antibunching in quantum beams. For this, in order to fit our experimental time scales, a single-photon source delivering at least one photon every 100 fs (on average) would be necessary (i.e., in the microwatt range for ≈1 eV photon). Moreover, it would be interesting to investigate an experimental situation in which there is less than one photon per mode (i.e., $\Phi \ll \Delta$ where Φ is the photon flux and Δ is the bandwidth, both in s^{-1}), for which important extrabunching effects [$g^{(2)}(0) \gg 3$] can be obtained [60]. Work is currently in progress to develop a TPC device with an enhanced two-photon detectivity allowing the investigation of such low photon fluxes.

ACKNOWLEDGMENTS

The authors want to thank Daniel I. Sessler, Professor and Chair, Department of Outcomes Research, Cleveland Clinic, and Professor Jacob Khurgin from Johns Hopkins University for critical reading of the manuscript.

APPENDIX A: ESTIMATION OF THE TPC YIELD IN GaAs

In order to estimate the quantum yield of TPC in GaAs, we will resort to the usual semiclassical approach in which the two-photon transition rate s_2 in a semiconductor detector is given by a quadratic law of the form

$$s_2 = q\beta \frac{P^2}{S}, \tag{A1}$$

where P is the incident light power, S is the light spot area on the photocathode, and β is the TPC coefficient. β (in $\text{cm}^2\,\text{W}^{-2}\,\text{s}^{-1}$) is related to the two-photon absorption coefficient α_2 (in cm W^{-1}) through the relation $\beta = \frac{\alpha_2 W}{\hbar\omega}$ where W is the effective space-charge layer width [47] and $\hbar\omega$ is the photon energy.

Assuming an ideal Gaussian beam, s_2 can be written as a function of the photocathode position z_d relative to the beam waist position:

$$s_2 = \beta \frac{P^2}{\pi w_0^2} \frac{1}{1 + (z_d/z_0)^2}, \tag{A2}$$

where $z_0 = \pi w_0^2/\lambda$ is the Rayleigh length, λ is the source wavelength (1.55 μm) and w_0 is the beam waist. Figure 9 shows a TPC Z scan [61] together with a theoretical fit by Eq. (A2). The agreement is excellent, indicating a coefficient β of 402 $\text{m}^2\,\text{W}^{-2}\,\text{s}^{-1}$ (i.e., $\alpha_2 \approx 10.25$ cm GW^{-1}) assuming a 1-μm effective collection length W. This value is somewhat smaller than the expected 15 cm GW^{-1} but little is known on

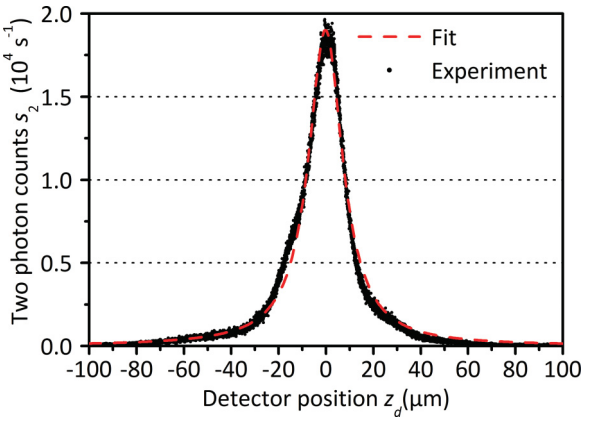

FIG. 9. (Color online) Variation of the TPC signal as a function of the detector position relative to the focus of a cw 1.55-μm laser diode. The result of this TPC Z scan experiment is fitted using Eq. (A2).

the collection efficiency in the space-charge layer, the emission efficiency of the electrons in the vacuum, and additional losses within the detector.

APPENDIX B: STOCHASTIC DESCRIPTION OF TWIN-PHOTON BEAMS

In Ref. [46], Loudon proposed the following definition of a nonclassical regime, involving the self- and cross-second-order correlations between beams:

$$\left|g_{si}^{(2)}(0)\right|^2 > \left|g_{ss}^{(2)}(0)\right|\left|g_{ii}^{(2)}(0)\right|. \tag{B1}$$

Since, in our experiments, the equality $|g_{si}^{(2)}(0)|^2 = |g_{ss}^{(2)}(0)||g_{ii}^{(2)}(0)| = 4$ applies, a description using the stochastic fluctuation of light is thus likely to take our results into account. The goal of this Appendix is to provide such a stochastic description.

We consider an assembly of n independent dipoles ($n \gg 1$) radiating at mean carrier frequencies ω_s and ω_i. In this way, the signal field can be written as

$$E_s(t) = E_{s,el}e^{-i\omega_s t}\sum_{j=1}^{n} e^{-i\varphi_{s,j}(t)}, \tag{B2}$$

where $\varphi_{s,j}(t)$ is the phase angle of an elementary signal field from the dipole j, which is completely unrelated to the other dipoles (as ones of a chaotic source) and $E_{s,el}$ is the elementary dipole field amplitude [46]. The idler field is given by a similar expression by replacing subscript s by i.

We shall start with the evaluation of the cross-correlation function $g_{si}^{(2)}(\tau)$:

$$\begin{aligned}&\langle I_s(t)I_i(t+\tau)\rangle \\ &\quad = E_{s,el}^4 e^{i(\omega_s-\omega_i)\tau}\left\langle\left|\sum_{j=1}^{n} e^{-i\varphi_{s,j}(t)}\right|^2\left|\sum_{j'=1}^{n} e^{-i\varphi'_{i,j}(t)}\right|^2\right\rangle.\end{aligned} \tag{B3}$$

The following derivation is based on the classical relation between the phases of parametrically mixed waves:

$$\varphi_{s,j}(t) + \varphi_{i,j}(t) = \varphi_{\text{pump}}(t) - \frac{\pi}{2}. \tag{B4}$$

This last expression describes the coherence between the idler and signal beams, enforced by the coherence of the pump $\varphi_{\text{pump}}(t) = \varphi_{\text{pump}}$. Using this latter relation in Eq. (B3), and neglecting the terms in n, one finds

$$\langle I_s(t)I_i(t+\tau)\rangle = n^2 I_{el}^2\left(1 + |\langle e^{-i[\varphi_{s,j}(t+\tau)+\varphi_{i,j}(t)]}\rangle|^2\right). \tag{B5}$$

Introducing the interbeam first-order correlation function,

$$\begin{aligned}g_{si}^{(1)}(\tau) &= \frac{\langle e^{i\omega_p t}E_s(t+\tau)E_i(t)\rangle}{\sqrt{I_i I_s}} \\ &= e^{-i\omega_s\tau}\langle\exp\{-i[\varphi_{s,j}(t+\tau)+\varphi_{i,j}(t)]\}\rangle,\end{aligned} \tag{B6}$$

Eq. (B5) also reads

$$g_{si}^{(2)}(\tau) = 1 + \left|g_{si}^{(1)}(\tau)\right|^2, \tag{B7}$$

which is similar to Eq. (31) derived in the frame of the quantum theory.

The second-order correlation function of the twin beams is now given by Eqs. (21)–(23) which still holds in this stochastic approach. We are left with evaluating the quantity $\text{Re}\langle e^{-i(\omega_i-\omega_s)\tau}E_s(t)E_s^*(t+\tau)E_i(t+\tau)E_i^*(t)\rangle$.

Using Eq. (B2), the quantity in brackets can be expanded as

$$\begin{aligned}&\langle e^{i(\omega_s-\omega_i)\tau}E_s(t)E_s^*(t+\tau)E_i(t)E_i^*(t+\tau)\rangle \\ &\quad = {E_{s,el}}^4 e^{i(\omega_s-\omega_i)\tau}\left\langle\left(\sum_{j=1}^{n} e^{-i\varphi_{s,j}(t)}\right)\left(\sum_{j'=1}^{n} e^{i\varphi_{s,j'}(t+\tau)}\right)\right. \\ &\qquad \left.\times\left(\sum_{j''=1}^{n} e^{i\varphi_{i,j''}(t)}\right)\left(\sum_{j'''=1}^{n} e^{-i\varphi_{i,j'''}(t+\tau)}\right)\right\rangle.\end{aligned} \tag{B8}$$

Using the correlation of Eq. (B4) and neglecting the terms in n, one finds

$$\begin{aligned}&\langle e^{i(\omega_s-\omega_i)\tau}E_s(t)E_s^*(t+\tau)E_i(t)E_i^*(t+\tau)\rangle \\ &\quad \approx n^2 I_{el}^2 e^{i(\omega_s-\omega_i)\tau}\langle e^{-i[\varphi_{s,j}(t)-\varphi_{s,j}(t+\tau)]}\rangle\langle e^{i[\varphi_{i,j}(t)-\varphi_{i,j}(t+\tau)]}\rangle \\ &\qquad + n^2 I_{el}^2 e^{i(\omega_s-\omega_i)\tau}\langle e^{-i[\varphi_{s,j}(t)+\varphi_{s,j}(t+\tau)]}\rangle\langle e^{i[\varphi_{i,j}(t)+\varphi_{i,j}(t+\tau)]}\rangle.\end{aligned} \tag{B9}$$

Considering the intrabeam first-order correlation functions given by [46],

$$\begin{aligned}g_{ss}^{(1)}(\tau) &\equiv \frac{\langle E_s(t)E_s*(t+\tau)\rangle}{\langle|E_s(t)|^2\rangle} \\ &= e^{-i\omega_s\tau}\langle\exp\{-i[\varphi_{s,j}(t)-\varphi_{s,j}(t+\tau)]\}\rangle, \\ g_{ii}^{(1)}(\tau) &\equiv \frac{\langle E_i(t)E_i*(t+\tau)\rangle}{\langle|E_i(t)|^2\rangle} \\ &= e^{-i\omega_i\tau}\langle\exp\{-i[\varphi_{i,j}(t)-\varphi_{i,j}(t+\tau)]\}\rangle,\end{aligned} \tag{B10}$$

Eq. (B9) finally leads to

$$\begin{aligned}&\text{Re}\langle e^{i(\omega_s-\omega_i)\tau}E_s(t)E_s^*(t+\tau)E_i(t)E_i^*(t+\tau)\rangle \\ &\quad = I_0^2\left[\left|g_{ss}^{(1)}(\tau)\right|\left|g_{ii}^{(1)}(\tau)\right| + \left|g_{si}^{(1)}(\tau)\right|^2\right]\cos(\omega_s-\omega_i)\tau.\end{aligned}$$

This last term $|g_{si}^{(1)}(\tau)|^2\cos(\omega_s-\omega_i)\tau$ would be missing if the idler and signal were not linked by the coherence condition of Eq. (B4).

Finally, from Eqs. (21)–(23), the second-order correlation function of the twin beams is given by

$$\begin{aligned}g^{(2)}(\tau) &= \tfrac{1}{4}\left[g_{ss}^{(2)}(\tau) + g_{ii}^{(2)}(\tau) + 2g_{si}^{(2)}(\tau)\right] \\ &\quad + \tfrac{1}{2}\left[\left|g_{ss}^{(1)}(\tau)\right|\left|g_{ii}^{(1)}(\tau)\right| + \left|g_{si}^{(1)}(\tau)\right|^2\right]\cos(\omega_s-\omega_i)\tau.\end{aligned} \tag{B11}$$

Let us assume that idler and signal beams are individually chaotic, i.e., $g_{ss}^{(2)}(\tau) = g_{ii}^{(2)}(\tau) = 1 + |g_{\text{chao.}}^{(1)}(\tau)|^2$. The second-order correlation function [Eq. (B11)] now reads

$$\begin{aligned}g^{(2)}(\tau) &= 1 + \frac{\left|g_{\text{chao.}}^{(1)}(\tau)\right|^2}{2}[1+\cos(\omega_s-\omega_i)\tau] \\ &\quad + \frac{\left|g_{si}^{(1)}(\tau)\right|^2}{2}[1+\cos(\omega_s-\omega_i)\tau].\end{aligned} \tag{B12}$$

This latter expression is consistent with Eqs. (21), (22), and (34) and exhibits all the main features observed in this study:

(i) The term "1" is the second-order function at very long delay when the fields have lost all their coherence properties.

(ii) The term $\frac{|g^{(1)}_{chao}(\tau)|^2}{2}[1+\cos(\omega_s-\omega_i)\tau]$ describes accidental coincidences. It provides the usual bunching behavior for incoherent beams. As already discussed in Sec. IV B 3, one could note that the oscillations exist even if the fields are not mutually coherent, which is experimentally observed.

(iii) The last term, $\frac{|g^{(1)}_{si}(\tau)|^2}{2}[1+\cos(\omega_s-\omega_i)\tau]$, exists only if the fields are mutually coherent. It describes exact coincidences between twin photons.

Finally one notes that at zero delay,

$$g^{(2)}(0)=2+\left|g^{(1)}_{si}(0)\right|^2, \tag{B13}$$

an expression which highlights the extrabunching effect when the beams are mutually coherent.

APPENDIX C: DERIVATION OF THE GENERALIZED EXPRESSION OF THE INTERBEAM CORRELATION FUNCTION OF TWIN BEAMS [EQ. (31)]

We start with the definition of the interbeam second-order correlation function according to Eq. (1):

$$g^{(2)}_{si}(\tau)=\frac{\langle\hat{a}^\dagger_i(t)\hat{a}^\dagger_s(t+\tau)\hat{a}_s(t+\tau)\hat{a}_i(t)\rangle}{\langle\hat{a}^\dagger_s(t)\hat{a}_s(t)\rangle\langle\hat{a}^\dagger_i(t)\hat{a}_i(t)\rangle}, \tag{C1}$$

where $\hat{a}_s(t)$ and $\hat{a}_i(t)$ are, respectively, defined in Eqs. (16) and (17). Let us first consider the numerator of Eq. (C1), i.e.,

$$\begin{aligned}\langle\hat{a}^\dagger_i(t)\hat{a}^\dagger_s(t+\tau)\hat{a}_s(t+\tau)\hat{a}_i(t)\rangle=&\frac{1}{4\pi^2}\int_0^{\omega_p 2}d\omega_1\int_{\omega_p/2}^{\omega_p}d\omega_2\int_{\omega_p/2}^{\omega_p}d\omega_3\int_0^{\omega_p/2}d\omega_4\,\eta(\omega_1)\eta(\omega_2)\eta(\omega_3)\eta(\omega_4)\\&\times\langle\hat{a}^\dagger(z_e,\omega_1)\hat{a}^\dagger(z_e,\omega_2)\hat{a}(z_e,\omega_3)\hat{a}(z_e,\omega_4)\rangle e^{i[\omega_1 t+\omega_2(t+\tau)-\omega_3(t+\tau)-\omega_4 t]}.\end{aligned} \tag{C2}$$

After substituting the operator $\hat{a}(z_e,\omega)$ by its expression as a function of crystal input operators $\hat{a}(\omega)$ and $\hat{a}^\dagger(\omega_p-\omega)$, i.e., Eq. (24), Eq. (C2) can be rewritten as follows:

$$\begin{aligned}\langle\hat{a}^\dagger_i(t)\hat{a}^\dagger_s(t+\tau)\hat{a}_s(t+\tau)\hat{a}_i(t)\rangle=&\frac{1}{4\pi^2}\int_0^{\omega_p/2}d\omega_1\int_{\omega_p/2}^{\omega_p}d\omega_2\int_{\omega_p/2}^{\omega_p}d\omega_3\int_0^{\omega_p/2}d\omega_4\,\eta^*(\omega_1)\eta^*(\omega_2)\eta(\omega_3)\eta(\omega_4)\\&\times\langle\nu^*(\omega_1)\hat{a}(\omega_{\rm p}-\omega_1)[\mu^*(\omega_2)\hat{a}^\dagger(\omega_2)-i\,\nu^*(\omega_2)\hat{a}(\omega_{\rm p}-\omega_2)]\\&\times[\mu(\omega_3)\hat{a}(\omega_3)+i\,\nu(\omega_3)\hat{a}^\dagger(\omega_{\rm p}-\omega_3)]\,\nu(\omega_4)\hat{a}^\dagger(\omega_{\rm p}-\omega_4)\rangle\\&\times e^{i\{[\omega_1 t+\omega_2(t+\tau)-\omega_3(t+\tau)-\omega_4 t]-[\Delta k(\omega_1)/2+k(\omega_1)+\Delta k(\omega_2)/2+k(\omega_2)-\Delta k(\omega_3)/2-k(\omega_3)-\Delta k(\omega_4)/2-k(\omega_4)]L\}}.\end{aligned} \tag{C3}$$

Using the operator commutation rule [Eq. (30)], Eq. (C3) yields

$$\begin{aligned}\langle\hat{a}^\dagger_i(t)\hat{a}^\dagger_s(t+\tau)\hat{a}_s(t+\tau)\hat{a}_i(t)\rangle=&\frac{1}{4\pi^2}\int_0^{\omega_p/2}d\omega_1\int_{\omega_p/2}^{\omega_p}d\omega_2\int_{\omega_p/2}^{\omega_p}d\omega_3\int_0^{\omega_p/2}d\omega_4\,\eta^*(\omega_1)\eta^*(\omega_2)\eta(\omega_3)\eta(\omega_4)\\&\times\nu^*(\omega_1)\nu(\omega_4)\{\mu^*(\omega_2)\mu(\omega_3)\delta(\omega_{\rm p}-\omega_1-\omega_2)\delta(\omega_{\rm p}-\omega_3-\omega_4)\\&+\nu^*(\omega_2)\nu(\omega_3)[\delta(\omega_1-\omega_3)\delta(\omega_2-\omega_4)+\delta(\omega_1-\omega_4)\delta(\omega_2-\omega_3)]\}\\&\times e^{i\{[\omega_1 t+\omega_2(t+\tau)-\omega_3(t+\tau)-\omega_4 t]-[\Delta k(\omega_1)/2+k(\omega_1)+\Delta k(\omega_2)/2+k(\omega_2)-\Delta k(\omega_3)/2-k(\omega_3)-\Delta k(\omega_4)/2-k(\omega_4)]L\}}.\end{aligned} \tag{C4}$$

Equation (C4) can then be rewritten as

$$\begin{aligned}\langle\hat{a}^\dagger_i(t)\hat{a}^\dagger_s(t+\tau)\hat{a}_s(t+\tau)\hat{a}_i(t)\rangle=&\left|\frac{i}{2\pi}\int_{\omega_p/2}^{\omega_p}d\omega\,\eta(\omega)\eta(\omega_{\rm p}-\omega)\nu(\omega)\mu(\omega)e^{-i\{\omega\tau-[\Delta k(\omega)+k(\omega)+k(\omega_{\rm p}-\omega)]L\}}\right|^2\\&+\left[\frac{1}{2\pi}\int_0^{\omega_p/2}d\omega|\eta(\omega)\nu(\omega)|^2\right]\left[\frac{1}{2\pi}\int_{\omega_p/2}^{\omega_p}d\omega|\eta(\omega)\nu(\omega)|^2\right].\end{aligned} \tag{C5}$$

Inserting Eq. (C5) into Eq. (C1) and using the definitions provided by Eqs. (25), (32), and (33), one straightforwardly recovers Eq. (31), i.e., $g^{(2)}_{si}(\tau)=1+|g^{(1)}_{si}(\tau)|^2$.

[1] R. Hanbury-Brown and R. Q. Twiss, Nature **177**, 27 (1956).

[2] H. Z. Cummins and E. R. Pike, *Photon Correlation Spectroscopy and Light Beating Spectroscopy* (Plenum Press, New York, 1974).

[3] Z. Zheng, A. M. Weiner, J. H. Marsh, and M. M. Karkhanehchi, IEEE Photonics Technol. Lett. **9**, 493 (1997).

[4] A. Migdall, Phys. Today **52**, 41 (1999).

[5] G. Ribordy, J. Brendel, J.-D. Gautier, N. Gisin, and H. Zbinden, Phys. Rev. A **63**, 012309 (2000).

[6] A. V. Sergienko, in *CXLVI International School of Physics "Enrico Fermi"*, edited by T. J. Quinn, S. Leschiutta, and P. Tavella (IOS Press, Amsterdam, 2001), pp. 715.

[7] Y. Tanaka, N. Sako, T. Kurokawa, H. Tsuda, and M. Takeda, Opt. Lett. **28**, 402 (2003).

[8] T. Liang, L. Nunes, T. Sakamoto, K. Sasagawa, T. Kawanishi, M. Tsuchiya, G. Priem, D. Van Thourhout, P. Dumon, R. Baets, and H. Tsang, Opt. Express **13**, 7298 (2005).

[9] J.-C. Diels and W. Rudolph, *Ultrashort Laser Pulse Phenomena* (Academic Press, Oxford, 2006).

[10] N. Gisin and R. Thew, Nat. Photonics **1**, 165 (2007).

[11] H. J. Kimble, Nature **453**, 1023 (2008).

[12] G. Baym, Acta Phys. Polonica B **29**, 1839 (1998).

[13] J. Viana-Gomes, D. Boiron, and M. Belsley, in *Strongly Correlated Systems, Coherence and Entanglement*, edited by J. Carmelo, J. Lopes dos Santos, V. R. Vieira, and P. D. Sacramento (World Scientific, Singapore, 2007), p. 335.

[14] N. Gisin, G. Ribordy, W. Tittel, and H. Zbinden, Rev. Mod. Phys. **74**, 145 (2002).

[15] E. Moreau, I. Robert, J. M. Gérard, I. Abram, L. Manin, and V. Thierry-Mieg, Appl. Phys. Lett. **79**, 2865 (2001).

[16] V. Zwiller, H. Blom, P. Jonsson, N. Panev, S. Jeppesen, T. Tsegaye, E. Goobar, M.-E. Pistol, L. Samuelson, and G. Björk, Appl. Phys. Lett. **78**, 2476 (2001).

[17] M. Beck, J. Opt. Soc. Am. B **24**, 2972 (2007).

[18] R. L. Byer and S. E. Harris, Phys. Rev. **168**, 1064 (1968).

[19] D. C. Burnham and D. L. Weinberg, Phys. Rev. Lett. **25**, 84 (1970).

[20] S. Friberg, C. K. Hong, and L. Mandel, Phys. Rev. Lett. **54**, 2011 (1985).

[21] I. Abram, R. K. Raj, J. L. Oudar, and G. Dolique, Phys. Rev. Lett. **57**, 2516 (1986).

[22] C. K. Hong, Z. Y. Ou, and L. Mandel, Phys. Rev. Lett. **59**, 2044 (1987).

[23] B. Dayan, A. Pe'er, A. A. Friesem, and Y. Silberberg, Phys. Rev. Lett. **93**, 023005 (2004).

[24] B. Dayan, A. Pe'er, A. A. Friesem, and Y. Silberberg, Phys. Rev. Lett. **94**, 043602 (2005).

[25] A. Pe'er, B. Dayan, A. A. Friesem, and Y. Silberberg, Phys. Rev. Lett. **94**, 073601 (2005).

[26] B. Dayan, Phys. Rev. A **76**, 043813 (2007).

[27] K. A. O'Donnell and A. B. U'Ren, Phys. Rev. Lett. **103**, 123602 (2009).

[28] S. Sensarn, G. Y. Yin, and S. E. Harris, Phys. Rev. Lett. **104**, 253602 (2010).

[29] A. Hayat, P. Ginzburg, and M. Orenstein, Opt. Express **17**, 21280 (2009).

[30] A. Hayat, A. Nevet, and M. Orenstein, Opt. Lett. **35**, 793 (2010).

[31] M. Aßmann, F. Veit, M. Bayer, M. van der Poel, and J. M. Hvam, Science **325**, 297 (2009).

[32] M. Aßmann, F. Veit, J.-S. Tempel, T. Berstermann, H. Stolz, M. van der Poel, J. M. Hvam, and M. Bayer, Opt. Express **18**, 20229 (2010).

[33] M. J. Stevens, B. Baek, E. A. Dauler, A. J. Kerman, R. J. Molnar, S. A. Hamilton, K. K. Berggren, R. P. Mirin, and S. Woo Nam, Opt. Express **18**, 1430 (2010).

[34] B. Blauensteiner, I. Herbauts, S. Bettelli, A. Poppe, and H. Hübel, Phys. Rev. A **79**, 63846 (2009).

[35] Y. Bromberg, Y. Lahini, E. Small, and Y. Silberberg, Nat. Photonics **4**, 721 (2010).

[36] J. Peřina, Jr., M. Hamar, and V. Michálek, Phys. Rev. A **85**, 023816 (2012).

[37] X. Gu, K. Huang, H. Pan, E. Wu, and H. Zeng, Opt. Express **20**, 2399 (2012).

[38] J. Gea-Banacloche, Phys. Rev. Lett. **62**, 1603 (1989).

[39] N. Ph. Georgiades, E. S. Polzik, K. Edamatsu, H. J. Kimble, and A. S. Parkins, Phys. Rev. Lett. **75**, 3426 (1995).

[40] N. P. Georgiades, E. S. Polzik, and H. J. Kimble, Phys. Rev. A **55**, R1605 (1997).

[41] Y. Takagi, T. Kobayashi, and K. Yoshihara, Opt. Lett. **17**, 658 (1992).

[42] F. Boitier, A. Godard, E. Rosencher, and C. Fabre, Nat. Phys. **5**, 267 (2009).

[43] F. Boitier, A. Godard, A. Ryasnyanskiy, N. Dubreuil, P. Delaye, C. Fabre, and E. Rosencher, Opt. Express **18**, 20401 (2010).

[44] F. Boitier, A. Godard, N. Dubreuil, P. Delaye, C. Fabre, and E. Rosencher, Nat. Commun. **2**, 425 (2011).

[45] B. R. Mollow, Phys. Rev. **175**, 1555 (1968).

[46] R. Loudon, *The Quantum Theory of Light* (Oxford University Press, Oxford, 2000).

[47] E. Rosencher and B. Vinter, *Optoelectronics* (Cambridge University Press, Cambridge, 2002).

[48] J. M. Roth, T. E. Murphy, and C. Xu, Opt. Lett. **27**, 2076 (2002).

[49] K. Mogi, K. Naganuma, and H. Yamada, Jpn. J. Appl. Phys. **27**, 2078 (1988).

[50] K. Kikuchi, Electron. Lett. **34**, 123 (1998).

[51] J. Brendel, E. Mohler, and W. Martienssen, Phys. Rev. Lett. **66**, 1142 (1991).

[52] P. G. Kwiat, W. A. Vareka, C. K. Hong, H. Nathel, and R. Y. Chiao, Phys. Rev. A **41**, 2910 (1990).

[53] J. G. Rarity, P. R. Tapster, E. Jakeman, T. Larchuk, R. A. Campos, M. C. Teich, and B. E. A. Saleh, Phys. Rev. Lett. **65**, 1348 (1990).

[54] A. Heidmann, R. J. Horowicz, S. Reynaud, E. Giacobino, C. Fabre, and G. Camy, Phys. Rev. Lett. **59**, 2555 (1987).

[55] B. Huttner, S. Serulnik, and Y. Ben-Aryeh, Phys. Rev. A **42**, 5594 (1990).

[56] F. Boitier, Ph.D. thesis, Ecole Polytechnique, Palaiseau, 2011.

[57] Z. Y. Ou and L. Mandel, Phys. Rev. Lett. **61**, 50 (1988).

[58] T. E. Keller and M. H. Rubin, Phys. Rev. A **56**, 1534 (1997).

[59] J. Liang, S. M. Hendrickson, and T. B. Pittman, Phys. Rev. A **83**, 033812 (2011).

[60] N. B. Grosse, T. Symul, M. Stobińska, T. C. Ralph, and P. K. Lam, Phys. Rev. Lett. **98**, 153603 (2007).

[61] M. Sheik-Bahae, A. A. Said, T. H. Wei, D. J. Hagan, and E. W. Van Stryland, IEEE J. Quantum Electron. **26**, 760 (1990).